













































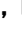




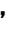

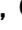


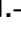
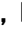












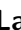












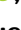





























































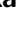

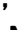




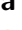




































































































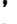
















































































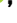



































PREPARED FOR SUBMISSION TO JHEP

Test of light-lepton universality in τ decays with the Belle II experiment

The Belle II Collaboration

I. Adachi , K. Adamczyk , L. Aggarwal , H. Aihara , N. Akopov , A. Aloisio , N. Anh Ky , D. M. Asner , H. Atmacan , V. Aushev , M. Aversano , R. Ayad , V. Babu , H. Bae , S. Bahinipati , P. Bambade , Sw. Banerjee , S. Bansal , M. Barrett , J. Baudot , A. Baur , A. Beaubien , F. Becherer , J. Becker , J. V. Bennett , F. U. Bernlochner , V. Bertacchi , M. Bertemes , E. Bertholet , M. Bessner , S. Bettarini , F. Bianchi , L. Bierwirth , T. Bilka , S. Bilokin , D. Biswas , A. Bobrov , D. Bodrov , A. Bolz , J. Borah , A. Boschetti , A. Bozek , M. Bračko , P. Branchini , T. E. Browder , A. Budano , S. Bussino , M. Campajola , L. Cao , G. Casarosa , C. Cecchi , J. Cerasoli , M.-C. Chang , P. Chang , R. Cheaib , P. Cheema , B. G. Cheon , K. Chilikin , K. Chirapatpimol , H.-E. Cho , K. Cho , S.-J. Cho , S.-K. Choi , S. Choudhury , L. Corona , J. X. Cui , S. Das , F. Dattola , E. De La Cruz-Burelo , S. A. De La Motte , G. de Marino , G. De Nardo , M. De Nuccio , G. De Pietro , R. de Sangro , M. Destefanis , S. Dey , R. Dhamija , A. Di Canto , F. Di Capua , J. Dingfelder , Z. Doležal , I. Domínguez Jiménez , T. V. Dong , M. Dorigo , D. Dorner , K. Dort , D. Dossett , S. Dreyer , S. Dubey , K. Dugic , G. Dujany , P. Ecker , M. Eliachevitch , D. Epifanov , P. Feichtinger , T. Ferber , D. Ferlewicz , T. Fillinger , C. Finck , G. Finocchiaro , A. Fodor , F. Forti , A. Frey , B. G. Fulsom , A. Gabrielli , E. Ganiev , M. Garcia-Hernandez , G. Gaudino , V. Gaur , A. Gaz , A. Gellrich , G. Ghevondyan , D. Ghosh , H. Ghumaryan , G. Giakoustidis , R. Giordano , A. Giri , A. Glazov , B. Gobbo , R. Godang , O. Gogota , P. Goldenzweig , W. Gradl , T. Grammatico , S. Granderath , E. Graziani , D. Greenwald , Z. Gruberová , T. Gu , Y. Guan , K. Gudkova , Y. Han , T. Hara , K. Hayasaka , H. Hayashii , S. Hazra , C. Hearty , M. T. Hedges , A. Heidelberg , I. Heredia de la Cruz , M. Hernández Villanueva , T. Higuchi , M. Hoek , M. Hohmann , P. Horak , C.-L. Hsu , T. Humair , T. Iijima , K. Inami , G. Inguglia , N. Ipsita , A. Ishikawa , R. Itoh , M. Iwasaki , W. W. Jacobs , D. E. Jaffe , E.-J. Jang , Q. P. Ji , S. Jia , Y. Jin , H. Junkerkalefeld , M. Kaleta , D. Kalita , A. B. Kaliyar , J. Kandra , S. Kang , G. Karyan , T. Kawasaki , F. Keil , C. Kiesling , C.-H. Kim , D. Y. Kim , K.-H. Kim , Y.-K. Kim , H. Kindo , K. Kinoshita , P. Kodyš , T. Koga , S. Kohani , K. Kojima , T. Konno , A. Korobov , S. Korpar , E. Kovalenko 

R. Kowalewski , T. M. G. Kraetzschmar , P. Križan , P. Krokovny , T. Kuhr , Y. Kulii , J. Kumar , M. Kumar , K. Kumara , T. Kunigo , A. Kuzmin , Y.-J. Kwon , S. Lacaprara , Y.-T. Lai , K. Lalwani , T. Lam , L. Lanceri , J. S. Lange , M. Laurenza , K. Lautenbach , R. Leboucher , F. R. Le Diberder , M. J. Lee , P. Leo , C. Lemettais , D. Levit , P. M. Lewis , C. Li , L. K. Li , S. X. Li , Y. Li , Y. B. Li , J. Libby , Z. Liptak , M. H. Liu , Q. Y. Liu , Y. Liu , Z. Q. Liu , D. Liventsev , S. Longo , T. Lueck , C. Lyu , Y. Ma , M. Maggiora , S. P. Maharana , R. Maiti , S. Maity , G. Mancinelli , R. Manfredi , E. Manoni , M. Mantovano , D. Marcantonio , S. Marcello , C. Marinas , C. Martellini , A. Martini , T. Martinov , L. Massaccesi , M. Masuda , K. Matsuoka , D. Matvienko , S. K. Maurya , J. A. McKenna , R. Mehta , F. Meier , M. Merola , F. Metzner , C. Miller , M. Mirra , S. Mitra , K. Miyabayashi , H. Miyake , R. Mizuk , G. B. Mohanty , S. Mondal , S. Moneta , H.-G. Moser , M. Mrvar , R. Mussa , I. Nakamura , K. R. Nakamura , M. Nakao , H. Nakazawa , Y. Nakazawa , A. Narimani Charan , M. Naruki , D. Narwal , Z. Natkaniec , A. Natochii , L. Nayak , M. Nayak , G. Nazaryan , M. Neu , C. Niebuhr , J. Ninkovic , S. Nishida , A. Novosel , S. Ogawa , Y. Onishchuk , H. Ono , F. Otani , P. Pakhlov , G. Pakhlova , A. Panta , S. Pardi , K. Parham , H. Park , S.-H. Park , B. Paschen , A. Passeri , S. Patra , T. K. Pedlar , R. Peschke , R. Pestotnik , M. Piccolo , L. E. Pilonen , G. Pinna Angioni , P. L. M. Podesta-Lerma , T. Podobnik , S. Pokharel , C. Praz , S. Prell , E. Prencipe , M. T. Prim , I. Prudiiev , H. Purwar , P. Rados , G. Raeuber , S. Raiz , N. Rauls , M. Reif , S. Reiter , M. Remnev , I. Ripp-Baudot , G. Rizzo , S. H. Robertson , M. Roehrken , J. M. Roney , A. Rostomyan , N. Rout , G. Russo , D. A. Sanders , S. Sandilya , L. Santelj , Y. Sato , V. Savinov , B. Scavino , C. Schmitt , C. Schwanda , M. Schwickardi , Y. Seino , A. Selce , K. Senyo , J. Serrano , M. E. Sevier , C. Sfienti , W. Shan , X. D. Shi , T. Shillington , J.-G. Shiu , D. Shtol , B. Shwartz , A. Sibidanov , F. Simon , J. B. Singh , J. Skorupa , R. J. Sobie , M. Sobotzik , A. Soffer , A. Sokolov , E. Solovieva , S. Spataro , B. Spruck , M. Starič , P. Stavroulakis , S. Stefkova , R. Stroili , Y. Sue , M. Sumihama , K. Sumisawa , W. Sutcliffe , N. Suwonjandee , H. Svidras , M. Takahashi , M. Takizawa , U. Tamponi , S. Tanaka , K. Tanida , F. Tenchini , A. Thaller , O. Tittel , R. Tiwary , D. Tonelli , E. Torassa , K. Trabelsi , I. Tsaklidis , M. Uchida , I. Ueda , T. Uglov , K. Unger , Y. Unno , K. Uno , S. Uno , P. Urquijo , Y. Ushiroda , S. E. Vahsen , R. van Tonder , K. E. Varvell , M. Veronesi , A. Vinokurova , V. S. Vismaya , L. Vitale , V. Vobbilisetti , R. Volpe , B. Wach , M. Wakai , S. Wallner , E. Wang , M.-Z. Wang , X. L. Wang , Z. Wang , A. Warburton , M. Watanabe , S. Watanuki , C. Wessel , E. Won , X. P. Xu , B. D. Yabsley , S. Yamada , W. Yan , S. B. Yang , J. Yelton , J. H. Yin , K. Yoshihara , C. Z. Yuan , Y. Yusa , L. Zani , F. Zeng , B. Zhang , Y. Zhang , V. Zhilich , Q. D. Zhou , X. Y. Zhou , V. I. Zhukova , R. Žlebčák

E-mail: coll-publications@belle2.org

ABSTRACT: We present a measurement of the ratio $R_\mu = \mathcal{B}(\tau^- \rightarrow \mu^- \bar{\nu}_\mu \nu_\tau) / \mathcal{B}(\tau^- \rightarrow e^- \bar{\nu}_e \nu_\tau)$ of branching fractions \mathcal{B} of the τ lepton decaying to muons or electrons using data collected with the Belle II detector at the SuperKEKB e^+e^- collider. The sample has an integrated luminosity of $362 \pm 2 \text{ fb}^{-1}$ at a centre-of-mass energy of 10.58 GeV. Using an optimised event selection, a binned maximum likelihood fit is performed using the momentum spectra of the electron and muon candidates. The result, $R_\mu = 0.9675 \pm 0.0007 \pm 0.0036$, where the first uncertainty is statistical and the second is systematic, is the most precise to date. It provides a stringent test of the light-lepton universality, translating to a ratio of the couplings of the muon and electron to the W boson in τ decays of 0.9974 ± 0.0019 , in agreement with the standard model expectation of unity.

KEYWORDS: e^+e^- Experiments, Tau Physics

ARXIV EPRINT: [2405.14625](https://arxiv.org/abs/2405.14625)

Contents

1	Introduction	1
2	The Belle II detector and simulation	2
3	Event selection	3
4	Method	7
5	Systematic uncertainties and consistency checks	8
5.1	Charged-particle identification	9
5.2	Imperfections of the simulation	10
5.3	Trigger	12
5.4	Size of the simulated samples and luminosity	13
5.5	Consistency checks	13
6	Results	14
7	Summary	15

1 Introduction

In the standard model (SM) of particle physics, lepton flavour universality (LFU) refers to an intrinsic property under which the electroweak gauge bosons have the same couplings to the three generations of leptons e , μ , and τ [1]. This symmetry originates from the fact that the only difference between lepton generations is derived from their distinct masses. A broad class of SM extensions postulates the existence of new particles, such as mediators of new interactions, that couple to the three leptons differently, making searches of LFU violation compelling [2, 3].

In the last decades, experimental tests of LFU have been carried out using various processes, but no significant deviation from the SM expectation has been observed. For example, tests in charged currents have been carried out in the decays of pions [4], kaons [5, 6], B mesons [7, 8], on-shell W bosons [9, 10], and τ leptons [11, 12]. Among these, the most precise LFU test is achieved in pion decays, followed by the τ -lepton decays, which are sensitive not only to charged currents but also to non-SM contributions of weak neutral currents [13, 14]. The LFU tests in τ decays rely on measurements of the τ mass, lifetime, and branching fractions of τ decays to lighter leptons or hadrons. The e - μ universality is tested by comparing the measured rates of leptonic τ decays, whose branching fractions are

denoted as $\mathcal{B}(\tau^- \rightarrow \mu^- \bar{\nu}_\mu \nu_\tau)$ and $\mathcal{B}(\tau^- \rightarrow e^- \bar{\nu}_e \nu_\tau)$. Charge-conjugate modes are implied throughout the paper. The ratio R_μ of the branching fractions,

$$R_\mu = \frac{\mathcal{B}(\tau^- \rightarrow \mu^- \bar{\nu}_\mu \nu_\tau)}{\mathcal{B}(\tau^- \rightarrow e^- \bar{\nu}_e \nu_\tau)}, \quad (1.1)$$

in turn, constrains the ratio of the effective coupling strengths g_e and g_μ of the electron and muon to the W^\pm ,

$$\left| \frac{g_\mu}{g_e} \right|_\tau = \sqrt{R_\mu \frac{f(m_e^2/m_\tau^2)}{f(m_\mu^2/m_\tau^2)}}. \quad (1.2)$$

Here $f(x) = 1 - 8x + 8x^3 - x^4 - 12x^2 \ln x$ under the assumption of negligible neutrino masses [1], and m_e , m_μ , and m_τ are the masses of the corresponding leptons. Thus, the challenge to test the e - μ universality is to accurately determine the ratio of branching fractions R_μ . This deviates from unity in the SM due to the difference in mass of the final state leptons and is predicted to be 0.9726. Previous measurements of R_μ were reported by the CLEO [11] and BaBar [12] collaborations. The most precise single determination of R_μ to date comes from the direct measurement of R_μ by the BaBar collaboration, $R_\mu = 0.9796 \pm 0.0016 \pm 0.0036$ [12], where the first uncertainty is statistical and the second is systematic. The measurement has 0.4% precision limited by the systematic uncertainties associated mainly with the lepton identification. This uncertainty propagates to 0.2% precision on $|g_\mu/g_e|_\tau = 1.0036 \pm 0.0020$. The current world average value of $|g_\mu/g_e|_\tau = 1.0019 \pm 0.0014$ [15] is consistent with unity, as predicted by the SM.

In this paper, we report a measurement of R_μ using data collected with the Belle II detector [16] at the energy-asymmetric e^+e^- SuperKEKB collider [17], with 7 GeV electron and 4 GeV positron beams colliding at 4.76° . The data were recorded between 2019 and 2022 at a centre-of-mass energy of 10.58 GeV and correspond to an integrated luminosity of $362 \pm 2 \text{ fb}^{-1}$ which translates to about 333×10^6 $e^+e^- \rightarrow \tau^+\tau^-$ events. We determine R_μ from events in which one τ decays either to $\tau^- \rightarrow e^- \bar{\nu}_e \nu_\tau$ or $\tau^- \rightarrow \mu^- \bar{\nu}_\mu \nu_\tau$, and the other τ decays hadronically. First, we optimise a selection that is common to both modes, after which we perform a binned maximum likelihood fit using the momentum spectra of the lepton candidates. All systematic effects are modelled directly in the likelihood function. Finally, we measure the value of R_μ from the fit and translate it into $|g_\mu/g_e|_\tau$, testing e - μ universality in charged current interactions.

2 The Belle II detector and simulation

The Belle II detector comprises several subdetectors arranged in a cylindrical structure around the e^+e^- interaction point [16]. Charged-particle trajectories (tracks) are reconstructed by a two-layer silicon-pixel detector, surrounded by a four-layer double-sided silicon-strip detector and a central drift chamber (CDC). Only 15% of the second pixel layer was installed when the data were collected. Outside the CDC, a time-of-propagation detector and an aerogel ring-imaging Cherenkov detector cover the barrel and forward endcap regions. The electromagnetic calorimeter (ECL), divided into the forward endcap, barrel, and

backward endcap, fills the remaining volume inside a 1.5 T superconducting solenoid and is used to reconstruct photons and electrons. A K_L^0 and muon detection system is installed in the iron flux return of the solenoid. The z axis of the laboratory frame is defined as the detector solenoid axis, with the positive direction along the electron beam. The polar angle θ and the transverse plane are defined relative to this axis.

Simulated samples are used for studying sample composition and optimising the analysis selections. We further rely on simulated samples to study and determine efficiencies and to define fit templates for the extraction of R_μ . Several processes contribute to the $e^+e^- \rightarrow \tau^+\tau^-$ sample as backgrounds, including $e^+e^- \rightarrow q\bar{q}$ events, where q indicates a u , d , s , or c quark; $e^+e^- \rightarrow e^+e^-(\gamma)$ and $\mu^+\mu^-(\gamma)$ events; $e^+e^- \rightarrow l^+l^-l^+l^-$ events, where l is a charged lepton; $e^+e^- \rightarrow e^+e^-h^+h^-$ events, where h indicates a pion or kaon; and $e^+e^- \rightarrow e^+e^-Nh$ events with multiplicity $N > 2$. We use several software packages to generate the simulated particles. The $e^+e^- \rightarrow \tau^+\tau^-$ process is generated using KKMC [18, 19], τ decays are simulated by TAUOLA [20–23] and their radiative corrections by PHOTOS [24]. We use KKMC to simulate $\mu^+\mu^-(\gamma)$ and $q\bar{q}$ production; PYTHIA [25] for the fragmentation of the $q\bar{q}$ pair; BabaYaga@NLO [26–30] for $e^+e^- \rightarrow e^+e^-(\gamma)$ events; and AAFH [31–33] and TREPS [34] for the production of non-radiative final states $l^+l^-l^+l^-$ and $e^+e^-h^+h^-$. Currently, there is no generator to simulate $e^+e^- \rightarrow e^+e^-Nh$ processes. The Belle II analysis software [35, 36] uses the GEANT4 [37] package to simulate the response of the detector to the passage of the particles.

3 Event selection

The trigger is based on ECL energy deposits (clusters) and their topologies in the ECL. The efficiency of the trigger system for this measurement is driven by the condition that the combined energy deposit of all ECL clusters exceeds 1 GeV. Events with two back-to-back clusters in the centre-of-mass system, one of which exceeds 4.5 GeV and the other 3 GeV, are vetoed by the trigger system to reject Bhabha events.

In the e^+e^- centre-of-mass frame, the τ leptons from $e^+e^- \rightarrow \tau^+\tau^-$ are produced in opposite directions and with a significant boost. Thus, the decay products of one τ are isolated from those of the accompanying τ and contained in opposite hemispheres. The boundary between those hemispheres is the plane perpendicular to the τ flight direction, which is experimentally approximated by the thrust axis. The thrust axis is the unit vector \hat{t} that maximizes the thrust value $\sum |\hat{t} \cdot \vec{p}_i^*| / \sum |\vec{p}_i^*|$, where \vec{p}_i^* is the momentum of the i th final state particle in the e^+e^- centre-of-mass frame [38, 39]. This calculation uses charged particles with the requirements given later in this section, as well as photons identified from clusters with energy above 150 MeV and within the CDC acceptance, having a polar angle θ of the momentum vector in the laboratory frame within $17^\circ < \theta < 150^\circ$ to ensure they are not matched to any charged particle. Throughout this paper, quantities in the e^+e^- centre-of-mass frame are indicated by an asterisk.

We define the *signal* hemisphere as the one containing a charged particle originating either from $\tau^- \rightarrow e^-\bar{\nu}_e\nu_\tau$ or $\tau^- \rightarrow \mu^-\bar{\nu}_\mu\nu_\tau$ decays. We also require that the opposite hemisphere, labelled with *tag*, contains only one charged particle and at least one neutral

pion. Thus, the tag side contains predominantly $\tau^+ \rightarrow h^+ n \pi^0 \bar{\nu}_\tau$ decays with multiplicity $n = 1, 2$.

We select τ -pair candidates by requiring the event to contain exactly two charged particles with zero total charge, each having a trajectory displaced from the average interaction point by less than 3 cm along the z axis and less than 1 cm in the transverse plane to reduce the contribution of misreconstructed or poorly constrained tracks. The charged particle on the tag side must satisfy the condition $E_{\text{ECL}}/p \leq 0.8 c$ to suppress electron contamination. Here, E_{ECL} denotes the energy deposit in the ECL, and p is the magnitude of the momentum vector of the associated particle. The charged particle on the signal side must be identified as either a muon or an electron according to the following conditions. Muons are identified using the discriminator $P_\mu = \mathcal{L}_\mu / (\mathcal{L}_e + \mathcal{L}_\mu + \mathcal{L}_\pi + \mathcal{L}_K + \mathcal{L}_p + \mathcal{L}_d)$ where the likelihood \mathcal{L} for each charged-particle hypothesis combines particle identification information from all detectors except the silicon trackers. Electrons are identified using a boosted decision tree classifier that is trained to separate electrons from all other charged particles [40]. This approach gives improved results compared to the purely likelihood-based approach, in particular for separating pions from electrons. Inputs to the classifier are the likelihoods from each sub-detector, as well as additional ECL observables, such as variables that characterise the cluster’s spatial structure. The most discriminating variable in the momentum range relevant to this analysis is E_{ECL}/p . We use the output of the classifier, P_e , as a discriminator for electron identification. We retain lepton candidates with requirements $P_e > 0.5$ and $P_\mu > 0.9$. We require that each lepton candidate, $\ell = e, \mu$ in the signal side satisfies the conditions $1.5 < p_\ell < 5 \text{ GeV}/c$, and $0.82 < \theta_\ell < 2.13 \text{ rad}$ to ensure accurate particle identification information. Here θ_ℓ refers to the polar angle of the momentum vector in the laboratory frame. While inefficiencies of the particle identification system are taken into account in our simulation, we correct for imperfections in the simulation using data-driven factors from calibration channels, as functions of momentum, polar angle, and charge. These channels are $J/\psi \rightarrow \ell^+ \ell^-$, $e^+ e^- \rightarrow \ell^+ \ell^- \gamma$, and $e^+ e^- \rightarrow e^+ e^- \ell^+ \ell^-$ events for efficiency, and $K_S^0 \rightarrow \pi^+ \pi^-$ and $e^+ e^- \rightarrow \tau^+ \tau^-$ events for misidentification rates. Due to limitations in calibration-sample sizes, events with candidate leptons $p_\ell > 4 \text{ GeV}/c$ and $\theta_\ell > 1.78 \text{ rad}$, or $p_\ell > 4.5 \text{ GeV}/c$ and $\theta_\ell > 1.16 \text{ rad}$ are vetoed. Electron and muon identification efficiencies are 99.7% and 93.9%, respectively. The rates for misidentifying pions as electrons or muons are 0.9% and 3.1%, respectively.

The momenta of charged particles are corrected for imperfections in the magnetic field description used for event reconstruction, misalignment of the detector, and material mis-modelling. The corresponding correction factor is evaluated by measuring the mass-peak position of a high-yield sample of $D^0 \rightarrow K^- \pi^+$ decays reconstructed in data and comparing this to the known value [41].

Neutral pions are identified as photon pairs with an invariant mass between $120 \text{ MeV}/c^2$ and $145 \text{ MeV}/c^2$, which is within two units of mass resolution from the known value. Those photons are identified from clusters, reconstructed within the CDC acceptance, $17^\circ < \theta < 150^\circ$, to ensure they are not matched to any charged particle. The energy threshold for selecting photon candidates varies based on the polar detector region, aiming to suppress beam-induced backgrounds. This adjustment is important for the endcaps where such backgrounds are more prominent. Specifically, we use 80 MeV for the forward region with $17^\circ < \theta < 31.4^\circ$,

30 MeV for the barrel with $32.2^\circ < \theta < 128.7^\circ$, and 60 MeV for the backward region with $130.7^\circ < \theta < 150^\circ$. The requirements $\alpha_{\gamma\gamma} < 1.4\text{rad}$ and $|\delta\phi| < 1.5\text{rad}$ on the angle α between the momenta of the two photons, and on the difference of azimuthal angles ϕ of the two photons reduce the combinatorial background from low-energy photons. The efficiency for identifying neutral pions with these criteria is 30 %.

The main background contamination comes from $e^+e^- \rightarrow e^+e^-(\gamma)$, $e^+e^- \rightarrow e^+e^-l^+l^-$ and $e^+e^- \rightarrow e^+e^-Nh$ processes. The $e^+e^- \rightarrow e^+e^-Nh$ events are suppressed using a data-driven selection. For these processes, the events are concentrated at low thrust values, at large values of the squared missing mass M_{miss}^2 , and at low missing transverse momentum $p_{T,\text{miss}}^*$. The missing momentum is the difference between the momenta of the initial e^+e^- and that of all reconstructed particles in the event, while the square of the missing mass is defined as $M_{\text{miss}}^2 = (\sqrt{s}/c^2 - E_{\text{vis}}^*/c^2)^2 - (p_{\text{miss}}^*/c)^2$, where E_{vis}^* is the energy of all reconstructed particles in the event and p_{miss}^* is the magnitude of the missing momentum vector. The $e^+e^- \rightarrow e^+e^-Nh$ background can be discriminated with these variables since the e^+e^- pair is not reconstructed and has a momentum vector parallel to the beam axis, while the remaining particles are not collinear. The requirements that the thrust value exceeds 0.85 and $M_{\text{miss}}^2 < (20\text{ GeV}^2/c^4 + 40\text{ GeV}/c^3 \cdot p_{T,\text{miss}}^*)$ are chosen to remove the contribution from the $e^+e^- \rightarrow e^+e^-Nh$ events.

For all other background processes, simulated signal and background events are used to train a neural network event classifier using cross-entropy as a loss function [42, 43]. The signal sample is defined as the combination of the $\tau^- \rightarrow e^-\bar{\nu}_e\nu_\tau$ and $\tau^- \rightarrow \mu^-\bar{\nu}_\mu\nu_\tau$ samples to have a common selection for both decays and, as a result, a cancellation of most of the systematic uncertainties on R_μ that are associated with the selection. Seven variables are used in the training: the thrust value, the polar angle of the thrust vector, E_{vis}^* , the transverse component of the missing momentum direction in the centre-of-mass frame, the momentum of the tag side charged particle and the invariant mass and polar angle of the $h^+n\pi^0$ system on the tag side in the centre-of-mass frame. We map them to four output nodes — one representing the combined electron and muon signal sample, the other three representing the various background events: $e^+e^- \rightarrow \tau^+\tau^-$ events with a misidentified signal or tag side, $e^+e^- \rightarrow e^+e^-$ events, and a combined sample of all remaining background events. The most discriminating variable is E_{vis}^* , which is twice as important as the least discriminating variable. Consistency checks with validation samples show no indication of overtraining. Figure 1 shows the output distribution of the neural network used to discriminate between $e^+e^- \rightarrow \tau^+\tau^-$ events with $\tau^- \rightarrow e^-\bar{\nu}_e\nu_\tau$ or $\tau^- \rightarrow \mu^-\bar{\nu}_\mu\nu_\tau$ decays on the signal side and all other events. The figure uses simulated training samples.

To select signal events, we require the output value of the neural network to be greater than 0.9, which yields the smallest total uncertainty on R_μ in simulation. The selected events are separated into electron and muon samples. These samples will be simultaneously fit in bins of the lepton candidate momentum in order to extract R_μ from the data. The momentum distributions of the electron and muon candidates in the simulated $\tau^- \rightarrow e^-\bar{\nu}_e\nu_\tau$ and $\tau^- \rightarrow \mu^-\bar{\nu}_\mu\nu_\tau$ samples, along with simulated background contributions, are shown in Figure 2. The distributions are corrected for imperfections in the simulation, in particular particle identification, the reconstruction of neutral particles, and trigger. The discontinuities at 4 GeV/c and 4.5 GeV/c in the distributions reflect the veto of events in certain lepton

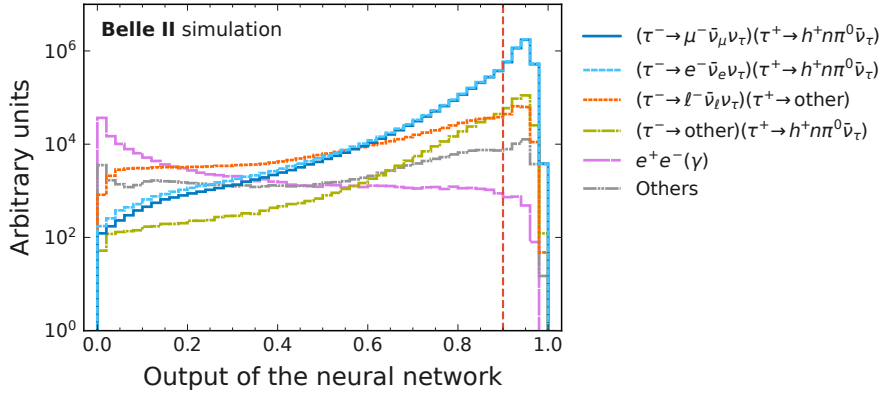


Figure 1. Distributions of the output of the neural network, trained to classify the combined sample of $\tau^- \rightarrow e^- \bar{\nu}_e \nu_\tau$ and $\tau^- \rightarrow \mu^- \bar{\nu}_\mu \nu_\tau$ decays. We show simulated background contributions from $e^+e^- \rightarrow \tau^+\tau^-$ events with decays other than $\tau^+ \rightarrow h^+ n \pi^0 \bar{\nu}_\tau$ on the tag side, with decays other than $\tau^- \rightarrow e^- \bar{\nu}_e \nu_\tau$ and $\tau^- \rightarrow \mu^- \bar{\nu}_\mu \nu_\tau$ on the signal side, and Bhabha events separately. The remaining background processes contributing to the spectrum are combined and collectively called ‘Others’. The dashed vertical line indicates the threshold used in this analysis.

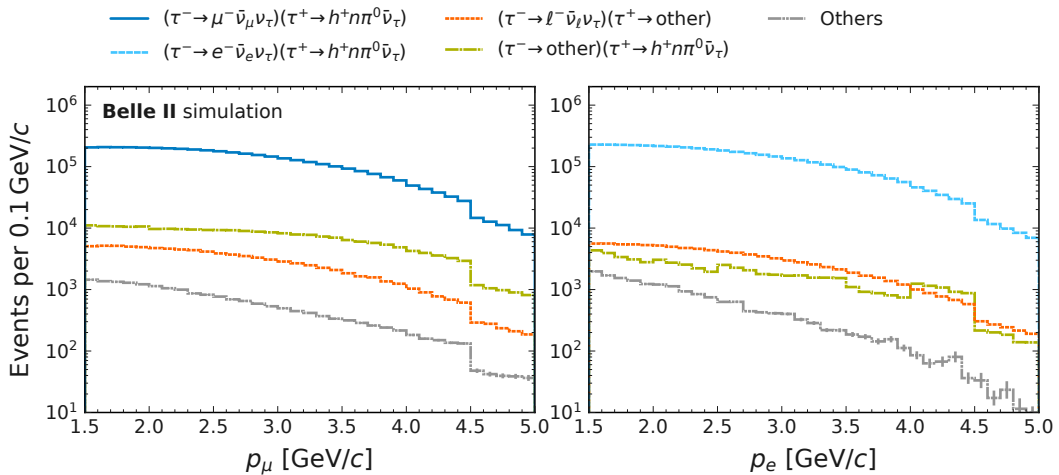


Figure 2. Momentum spectra of muon (left) and electron (right) candidates from simulated $\tau^- \rightarrow \mu^- \bar{\nu}_\mu \nu_\tau$ and $\tau^- \rightarrow e^- \bar{\nu}_e \nu_\tau$ samples, along with simulated background contributions. The legend uses a similar nomenclature as Figure 1.

identification correction bins as well as the impact of the correction factors themselves.

The trigger efficiency is measured with a reference sample selected by independent triggers based on the number of particles reconstructed in the CDC. The trigger efficiency in data is 99.8% for $\tau^- \rightarrow e^- \bar{\nu}_e \nu_\tau$ and 96.6% for $\tau^- \rightarrow \mu^- \bar{\nu}_\mu \nu_\tau$ decays, which is primarily driven by the tag hemisphere. In simulation, the corresponding efficiencies are 98.6% and 95.4%, respectively. To account for imperfection in the simulation of the trigger, we apply correction factors as ratios of efficiencies in data and simulation to our simulated samples. The correction factors are stable as a function of the lepton candidate momentum and independent of the flavour of the signal lepton.

The signal-reconstruction efficiency in simulation after all selection requirements and applied corrections is 9.602% for $\tau^- \rightarrow e^- \bar{\nu}_e \nu_\tau$ and 9.551% for $\tau^- \rightarrow \mu^- \bar{\nu}_\mu \nu_\tau$. The purity is 96% for the e -sample and 92% for the μ -sample. The dominant backgrounds are from $e^+e^- \rightarrow \tau^+\tau^-$ events with $\tau^- \rightarrow h^- \nu_\tau$ or $\tau^- \rightarrow h^- n\pi^0 \nu_\tau$ decays in the signal hemisphere, which makes up 1.3% of the e -sample and 5.2% of the μ -sample. This is followed by 2.3% of $e^+e^- \rightarrow \tau^+\tau^-$ events with a misidentified tag side decay and 0.2% of $e^+e^- \rightarrow e^+e^- \tau^+\tau^-$ events, for both samples. In data, we observe 4 371 737 events for which the lepton candidate is identified as a muon and 4 358 376 events for which it is identified as an electron.

4 Method

To determine signal yields we use the *pyhf* package [44], which constructs a binned likelihood following the HistFactory [45] formalism. The templates for the signal and background momentum distributions are derived from simulation and use 21 bins spanning the lepton candidate momentum. We apply data-driven corrections to these templates that account for imperfect simulation of particle identification, neutral particle reconstruction, and trigger efficiency. This binning choice is derived from the lepton identification correction bins. The momentum range is covered by seven bins with a bin width of 0.5 GeV/ c , which are further split into three equal-sized bins to define the templates. The events are separated into channels according to the previously specified lepton identification criteria. For each channel, one template represents the signal component, and two templates describe the backgrounds, separated into events with correctly identified leptons and all other background events. Systematic uncertainties are incorporated with multiplicative or additive event-count modifiers in the likelihood. The likelihood function f is a product of Poisson probability density functions \mathcal{P} that combines the information from all bins of signal and background samples,

$$f(R_\mu, \vec{\chi}) = \prod_{b \in \text{bins}} \mathcal{P}(n_b^e | \nu_b^e(\vec{\chi})) \prod_{b \in \text{bins}} \mathcal{P}(n_b^\mu | \nu_b^\mu(R_\mu, \vec{\chi})) \prod_{\chi \in \vec{\chi}} c_\chi(a_\chi | \chi). \quad (4.1)$$

Here, n_b^e and n_b^μ are the number of observed $\tau^- \rightarrow e^- \bar{\nu}_e \nu_\tau$ and $\tau^- \rightarrow \mu^- \bar{\nu}_\mu \nu_\tau$ candidate events in data for each bin b of the template. The corresponding expected number of events from simulations are denoted as ν_b^e and ν_b^μ . The systematic uncertainties discussed below are included in the likelihood as a set of nuisance parameters $\vec{\chi}$ that are event-count modifiers, constrained by normal probability density functions c_χ associated with auxiliary data a_χ . We model each momentum spectrum as a sum of contributions from the signal $\tau^- \rightarrow e^- \bar{\nu}_e \nu_\tau$ or $\tau^- \rightarrow \mu^- \bar{\nu}_\mu \nu_\tau$ decays and all sources of background events. Since the majority of the background originates from $e^+e^- \rightarrow \tau^+\tau^-$ events, we do not split the background templates according to the physics processes. Instead, we distinguish them by the signal side particle type in order to separate the effects of the uncertainties associated with lepton identification and misidentification on the templates. The resulting expressions for the expected events for each bin are

$$\nu_b^e(\vec{\chi}) = \kappa_e \nu_b^{e\text{-sig}}(\vec{\chi}) + \nu_b^{e\text{-bkg(true)}}(\vec{\chi}) + \nu_b^{e\text{-bkg(fake)}}(\vec{\chi}) \text{ and} \quad (4.2)$$

$$\nu_b^\mu(R_\mu, \vec{\chi}) = R_\mu \kappa_{e/\mu}^{\text{gen}} \kappa_e \nu_b^{\mu\text{-sig}}(\vec{\chi}) + \nu_b^{\mu\text{-bkg(true)}}(\vec{\chi}) + \nu_b^{\mu\text{-bkg(fake)}}(\vec{\chi}) . \quad (4.3)$$

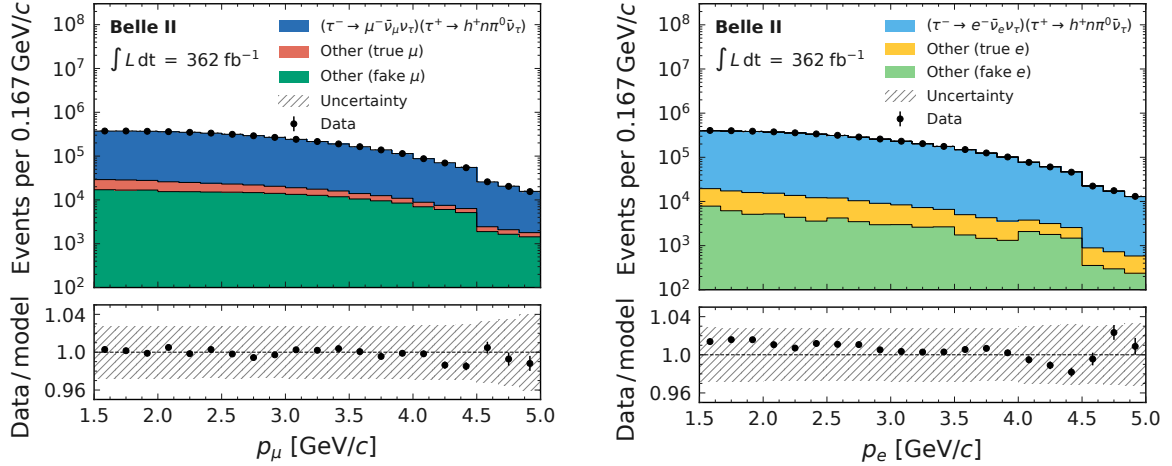


Figure 3. Observed momentum distribution for muon (left) and electron (right) candidates with simulation expectations overlaid. The lower panel shows the ratio between data and expectations with systematic uncertainties (hatched).

Here $\nu_b^{e\text{-sig}}$ and $\nu_b^{\mu\text{-sig}}$ are the signal yields, $\nu_b^{e\text{-bkg(true)}}$ and $\nu_b^{\mu\text{-bkg(true)}}$ are the yields of background events with the particle in the signal side properly identified as either an electron or a muon, and $\nu_b^{e\text{-bkg(fake)}}$ and $\nu_b^{\mu\text{-bkg(fake)}}$ stand for the remaining background events, mostly with pions misidentified as leptons. The factor κ_e , which is free in the fit, sets the overall normalisation of the signal templates; the constant scaling factor $\kappa_{e/\mu}^{\text{gen}} \equiv \mathcal{B}_e^{\text{gen}}/\mathcal{B}_\mu^{\text{gen}}$ takes the assumed branching fractions from the simulation into account. This allows the ratio R_μ to be estimated directly from the fit: it is determined simultaneously along with the nuisance parameters by maximising the likelihood function. Figure 3 shows the yields from experimental data, superimposed with the expected yields from simulation. The hatched area in the lower panel indicates the possible variation of the yields due to systematic effects, with the dominant contribution being the π^0 efficiency uncertainty.

To minimise the observer-expectancy effect, we validate the R_μ measurement method using simulation, and estimate the statistical and systematic uncertainties using data without examining the central value of the result. This is achieved by randomly adjusting the values of branching fractions $\mathcal{B}_e^{\text{gen}}$ and $\mathcal{B}_\mu^{\text{gen}}$ used in the generation within a 2% range. This allows us to validate the fit and the shapes of all distributions without observing the actual value.

5 Systematic uncertainties and consistency checks

The systematic uncertainties are grouped into categories associated with charged-particle identification, imperfections of the simulation, trigger, size of the simulated samples, and luminosity. We include one or more nuisance parameters for each systematic source depending on the correlations between the individual template bins. The nuisance parameters modify the event-counts of the templates to capture the impact of each systematic uncertainty on the observed momentum distribution of the leptons. The total number of nuisance parameters in the fit amounts to 194. Table 1 summarises the sources contributing to the total uncertainty on R_μ . To estimate the uncertainty of each contribution, we generate 2000 simulated

Source	Uncertainty [%]
Charged-particle identification:	0.32
Electron identification	0.22
Muon misidentification	0.19
Electron misidentification	0.12
Muon identification	0.05
Imperfections of the simulation:	0.14
Modelling of FSR	0.08
Normalisation of individual processes	0.07
Modelling of the momentum distribution	0.06
Tag side modelling	0.05
π^0 efficiency	0.02
Particle decay-in-flight	0.02
Tracking efficiency	0.01
Modelling of ISR	0.01
Photon efficiency	< 0.01
Photon energy	< 0.01
Detector misalignment	< 0.01
Momentum correction	< 0.01
Trigger	0.10
Size of the simulated samples	0.06
Luminosity	0.01
Total	0.37

Table 1. Fractional systematic uncertainty on R_μ , split into the contributing sources. The total fractional systematic uncertainty is 0.37 %, translating into an absolute uncertainty of 0.0036.

replicas of data by sampling the likelihood, where only auxiliary data associated with the respective nuisance parameters are varied according to the associated constraint terms. The standard deviation of the resultant distribution of fitted R_μ values is quoted as the size of the corresponding systematic effect. The largest uncertainty on R_μ arises from the particle identification. The total absolute systematic uncertainty on R_μ is 0.0036.

5.1 Charged-particle identification

Systematic uncertainties associated with charged-particle identification are obtained from data-driven corrections to the lepton identification efficiencies and particle misidentification rates in simulation. The corrections and their uncertainties are summarised in Table 2. The uncertainties of the correction factors have statistical and systematic components. The statistical uncertainties are dominant for the muon identification corrections and are included in the fit model as fully independent across all correction bins. Systematic components dominate the uncertainties of the electron identification corrections. The systematic uncertainties are assumed to be fully correlated across the correction bins, which is demonstrated

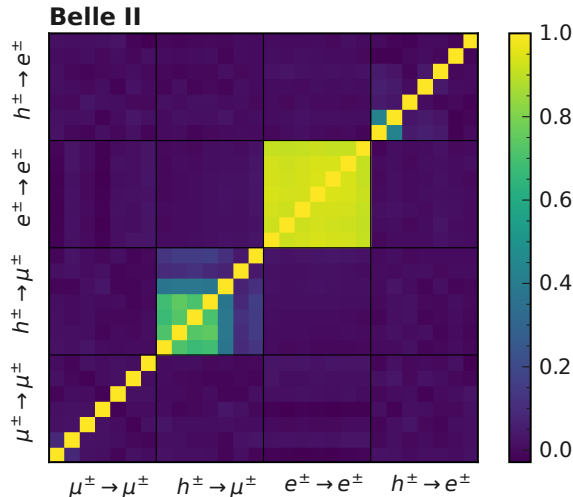


Figure 4. Correlations between the correction uncertainties of the lepton efficiencies ($\mu^\pm \rightarrow \mu^\pm$, $e^\pm \rightarrow e^\pm$) and misidentification rates ($h^\pm \rightarrow \mu^\pm$, $h^\pm \rightarrow e^\pm$). Each block for every category shows the correlation between the individual momentum bins.

in simplified simulated experiments to be the most conservative approach. If the uncertainty is asymmetric, the larger of the signed variations is considered for both. The resulting correlations between the individual template bins are shown in Figure 4. The efficiency correction uncertainties are applied to the templates with true leptons of the same type. Meanwhile, misidentification rate uncertainties are applied to the templates with the fake leptons. Since the corrections are binned in steps of 0.5 GeV in momentum, only 7 parameters are required to model the uncertainties associated with efficiencies and misidentification rates, respectively. This results in a total of 28 nuisance parameters. The relative uncertainty on R_μ associated with charged-particle identification is 0.32%, shared between the muon and electron identification and misidentification uncertainties.

	Correction range	Average correction	Uncertainty range [%]	Average uncertainty [%]
Electron identification	0.99 to 1.01	1.00	0.05 to 1.35	0.22
Muon identification	0.87 to 0.99	0.97	0.10 to 6.00	0.38
Electron misidentification	1.00 to 13.0	2.61	3.54 to 162	41.4
Muon misidentification	0.25 to 1.10	0.82	3.11 to 76.9	11.7

Table 2. Ranges and average values for the correction factors and associated total uncertainties of the lepton identification efficiencies, and the rates of pions misidentified as leptons. The uncertainties are given relative to the correction factors.

5.2 Imperfections of the simulation

Any mismodelling of the simulation that affects both the electron and the muon momentum distributions equally would cancel in measuring R_μ . We examine potential simulation mismodellings that could impact the momentum distributions of electrons and muons in

$\tau^- \rightarrow e^- \bar{\nu}_e \nu_\tau$ and $\tau^- \rightarrow \mu^- \bar{\nu}_\mu \nu_\tau$ decays or one of the backgrounds differently. Specifically, modelling of initial and final state radiation (ISR and FSR), and the reconstruction efficiency of radiated photons may differ in simulated samples and data. We modify the number of events with an ISR photon by varying them from 5% to 20%. The resulting effect on R_μ is approximately 0.01% for all variations, since ISR largely cancels because it has a similar effect on all templates. This is not true for FSR, which also includes bremsstrahlung photons, since the effect on the momentum of the electron in $\tau^- \rightarrow e^- \bar{\nu}_e \nu_\tau$ is expected to be larger than that of the muon in $\tau^- \rightarrow \mu^- \bar{\nu}_\mu \nu_\tau$. To account for the possibility of misestimating the number of FSR photons in the simulation compared to data, we randomly select 5% of the generated FSR photons in simulation and add their momenta to the momentum of the corresponding lepton. This fraction of added FSR momenta is based on a study with $J/\psi \rightarrow e^+e^-$ and $J/\psi \rightarrow \mu^+\mu^-$ samples, with the second as a control mode not sensitive to radiative effects in the final state. Agreement within 5% is observed between simulations and data for the control samples in the distribution of the energy recovered as FSR from electrons. The resulting template variations of the lepton momentum distributions are symmetrised to also account for the possible underestimation of the number of FSR photons in the simulation. The systematic uncertainty arising from the potential mismodelling of FSR propagated to R_μ is estimated to be 0.08%.

Systematic effects may emerge due to the differences in the normalisations of the underlying physics processes. Here, we independently consider variations in the yields of $e^+e^- \rightarrow \tau^+\tau^-$ events with a misidentified signal side, with a misidentified tag side, as well as the yields of non-taupair background processes. In addition, we vary the total $e^+e^- \rightarrow \tau^+\tau^-$ yield given the uncertainty of the $e^+e^- \rightarrow \tau^+\tau^-$ cross section and the uncertainties of the tag side branching fractions. We assess the effect of these normalisation differences by re-computing the templates with the varied yields. The resulting variations are included in the model, where each independent variation is parametrised by one nuisance parameter. The corresponding systematic uncertainty on R_μ is 0.07%.

To account for possible simulation mismodelling that could alter the shape of the templates, we add uncertainties to each template bin that are fully correlated across all six templates but only affect one momentum bin at a time, resulting in 21 nuisance parameters. The size of this uncertainty is estimated in a data-driven manner by analysing the spread of the ratio between data and simulations of a sample without any particle identification requirement imposed on the signal side. We use the standard deviation of this ratio, computed in the 21 momentum bins of the templates, which amounts to 0.84%. This results in an overall effect on R_μ of 0.06%.

Using an *embedding* technique on the combined sample of $\tau^- \rightarrow e^- \bar{\nu}_e \nu_\tau$ and $\tau^- \rightarrow \mu^- \bar{\nu}_\mu \nu_\tau$ events, both in simulations and in data, we study possible simulation mismodellings of the tag side that might affect the event selection. We select the electron or muon candidate in each event and replace it with a randomly selected lepton from the simulated $\tau^- \rightarrow e^- \bar{\nu}_e \nu_\tau$ or $\tau^- \rightarrow \mu^- \bar{\nu}_\mu \nu_\tau$ events. To ensure a reasonable match, we perform these replacements in quintiles of the lepton momentum, selecting charged particles with momentum magnitudes similar to the original lepton. We then adjust the momentum direction of the replaced particle to align with the original momentum direction. Additionally, all variables affected by the replaced lepton momentum are recalculated accordingly. The observed differences of the

resulting data-over-simulation ratios between the embedded $\tau^- \rightarrow e^- \bar{\nu}_e \nu_\tau$ and $\tau^- \rightarrow \mu^- \bar{\nu}_\mu \nu_\tau$ events are around 0.2%, depending on the momentum of the lepton candidate. Since the same $\tau^- \rightarrow e^- \bar{\nu}_e \nu_\tau$ or $\tau^- \rightarrow \mu^- \bar{\nu}_\mu \nu_\tau$ events are embedded in data and simulated samples, any differences are expected to arise solely from the tag side. These differences are small and consistent with statistical fluctuations, but to be conservative they are included in the fit model as fully uncorrelated variations of the template bins with 42 nuisance parameters and contribute a 0.05% uncertainty on R_μ .

The correction of neutral pion reconstruction efficiency, to account for differences between simulation and data, is determined as a function of the pion momentum from auxiliary measurements in calibration channels of D and τ decays. The impact of the uncertainty of this correction on R_μ is estimated to be 0.02%.

To estimate the impact of mismodelled charged-particle decay-in-flight rates in simulations, we modify the number of tracks reconstructed from the decay products of other particles, primarily pions, by 5%. The mismodelling of tag side pion decays affects the muon and electron templates similarly, leading to a cancellation of the systematic effects. However, the signal side muon templates would be affected significantly by the modification in pion decay rates, and the effect does not cancel out. The associated systematic uncertainty on R_μ is 0.02%.

Differences between the track finding efficiencies in simulation and data have been measured in $e^+e^- \rightarrow \tau^+\tau^-$ events with one of the τ leptons decaying to three charged hadrons. A per-track systematic uncertainty of 0.24% is included as a normalisation uncertainty of the templates to account for these differences. The associated systematic uncertainty on R_μ is 0.01%.

Systematic uncertainties due to simulation mismodelling of the detection efficiency of photons and their energies, detector misalignment, and charged-particle momentum correction are each found to be below 0.01%.

5.3 Trigger

The template yields in each bin are corrected to account for differences in trigger efficiency between data and simulation. The average of the correction factors that are applied to the simulated events is 1.0122 for the muon channel and 1.0125 for the electron channel. Several uncertainties are associated with this correction, summarised in Table 3. They include statistical uncertainties from the measured efficiency in data and simulation, and systematic uncertainties associated with the efficiency estimation method. For the systematic effects, we consider the potential bias introduced if the CDC triggers used to define the reference sample in which the efficiency is measured are not completely independent from the ECL triggers. This potential bias is obtained from simulation by comparing the efficiency calculated in the reference sample to the absolute efficiency for the entire sample. In addition, we consider the observed differences in the correction factors when computed with an alternative reference sample with additional CDC triggers used to obtain it. The latter is the dominant source of uncertainty. The uncertainties from the various sources are combined in quadrature for each bin and included in the fit model with 44 nuisance parameters under the assumption of independence across momentum bins and between the electron and muon channels. This assumption is conservative, since most systematic effects originate from a common source for

both channels, which causes a cancellation of the effect when measuring R_μ . In particular, the changes in the correction factors when computed with alternative reference triggers are similar for both channels, which indicates a high correlation. However, some independent effects can still arise due to differences in lepton flavour on the signal hemisphere. This motivates the more conservative choice of independent uncertainties. The systematic uncertainty propagating to R_μ is determined to be 0.10 %.

	μ channel		e channel	
	Range [%]	Average [%]	Range [%]	Average [%]
Sample size	0.04 to 0.23	0.05	0.01 to 0.08	0.02
Absolute efficiency	0.00 to 0.10	0.07	-0.11 to 0.01	-0.01
Alternative reference triggers	0.09 to 0.20	0.15	0.09 to 0.15	0.13

Table 3. Range and average of the uncertainties associated with the trigger correction. The first row shows the statistical uncertainties, while the other two rows show the uncertainties attributed to systematic effects, as mentioned in the text. The uncertainties are given relative to the correction factors. The systematic uncertainties are obtained from differences with respect to the nominal correction, the direction of which is given by the sign.

5.4 Size of the simulated samples and luminosity

The templates are allowed to vary due to the limited size of the simulated samples, which is parametrised by one nuisance parameter per bin. The extent of this variation is mainly affected by the size of the simulated $e^+e^- \rightarrow \tau^+\tau^-$ sample, which is 1 ab^{-1} . The resulting systematic uncertainty on R_μ is 0.06 %.

Since the uncertainty on the luminosity measurement affects all distributions, its impact on R_μ largely cancels. It does not entirely vanish since the overall change in normalisation of the templates can also be related to a combination of other systematic effects, which in turn can affect R_μ . This is a very small effect and of the order of 0.01 %.

5.5 Consistency checks

We check the stability of the result throughout various data-taking periods and observe no evidence of time dependence. We also determine that the value of R_μ is consistent when varying the event classifier neural network threshold within 0.05 around the nominal requirement. To exclude a potential dependence of the measured R_μ on the properties of the electrons and muons, we divide the data into sub-regions of various variables. Specifically, we use the lepton charge (q_ℓ), momentum, and polar angle. Another split of the sample is performed using the polar angle of the missing momentum vector (θ_{miss}). To rule out potential dependence on the particle identification requirements, we check the stability of the results using different requirements on the particle identification discriminators P_e and P_μ . Namely, we use $P_e = 0.90, 0.95, 0.99$ and $P_\mu = 0.50, 0.95, 0.99$ and compare the results to those obtained with the nominal requirements. We also check the stability of the result when changing the assumed correlation of lepton identification systematic uncertainties (ρ_{LID}) and the number of bins used to define the templates. The outcome of some of these checks is shown in Figure 5, where the shaded area indicates the statistical uncertainty, while the

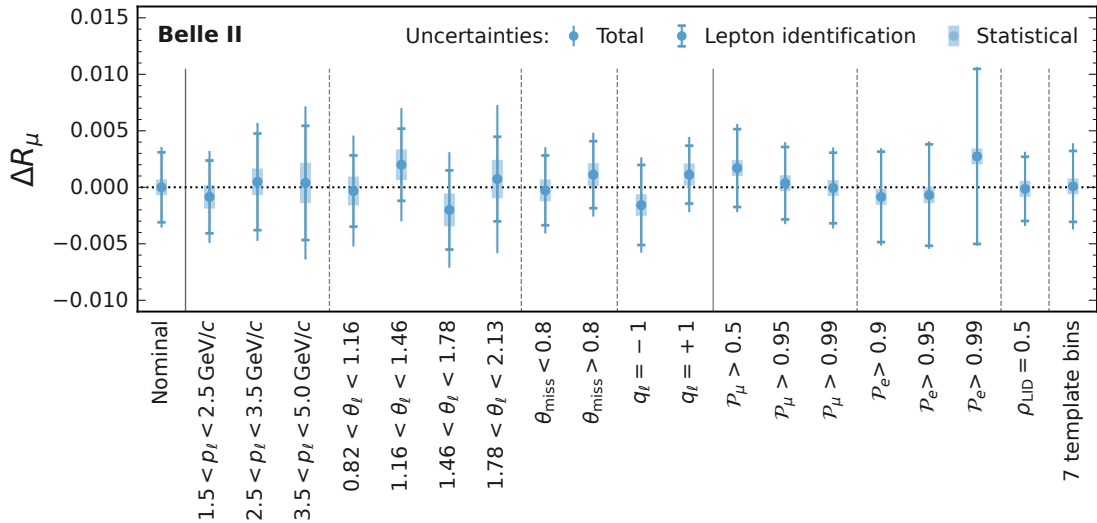


Figure 5. Stability of the fitted value of R_μ . Shown are deviations ΔR_μ from the nominal value for different sub-regions of selected variables, for different requirements on the particle identification discriminators, and for different fit conditions. The measurements in each sub-region are statistically independent in the first four groups, separated by dashed vertical lines.

error cap marks the systematic uncertainty originating only from lepton identification, and the error bars show the total uncertainties. We obtain consistent results from all performed checks, indicating no significant unaccounted-for systematic effects.

6 Results

The distribution of the muon and electron candidate momentum with fit results overlaid is shown in Figure 6. We measure the ratio of branching fractions

$$R_\mu = \frac{\mathcal{B}(\tau^- \rightarrow \mu^- \bar{\nu}_\mu \nu_\tau)}{\mathcal{B}(\tau^- \rightarrow e^- \bar{\nu}_e \nu_\tau)} = 0.9675 \pm 0.0007 \pm 0.0036. \quad (6.1)$$

The first uncertainty is statistical, while the second uncertainty is systematic. The statistical uncertainty is determined by performing the fit with all nuisance parameters fixed to their best-fit values, and the systematic component is calculated by subtraction in quadrature from the total uncertainty obtained with the nominal fit. This is consistent with the systematic uncertainty obtained in Table 1. The dominant source of systematic uncertainty is lepton identification. The measured normalisation yields are $4\,156\,500 \pm 99\,650$ for $\tau^- \rightarrow e^- \bar{\nu}_e \nu_\tau$ and $4\,000\,190 \pm 99\,260$ for $\tau^- \rightarrow \mu^- \bar{\nu}_\mu \nu_\tau$, with a correlation of 0.988. The dominant source of uncertainty in the yield estimates is related to the π^0 reconstruction efficiency, which only affects the tag side. The value of R_μ obtained is shown in the left panel of Figure 7 and compared to previous measurements performed by CLEO [11] and BaBar [12] as well as the global determination from a fit to all τ branching fractions [15]. Our result is consistent with previous measurements and is the most precise measurement from a single experiment to date. Using Equation 1.2, we translate the measured R_μ value into the most stringent test of LFU in τ -lepton decays from a single experiment, obtaining $|g_\mu/g_e|_\tau = 0.9974 \pm 0.0019$ (see the right panel of Figure 7).

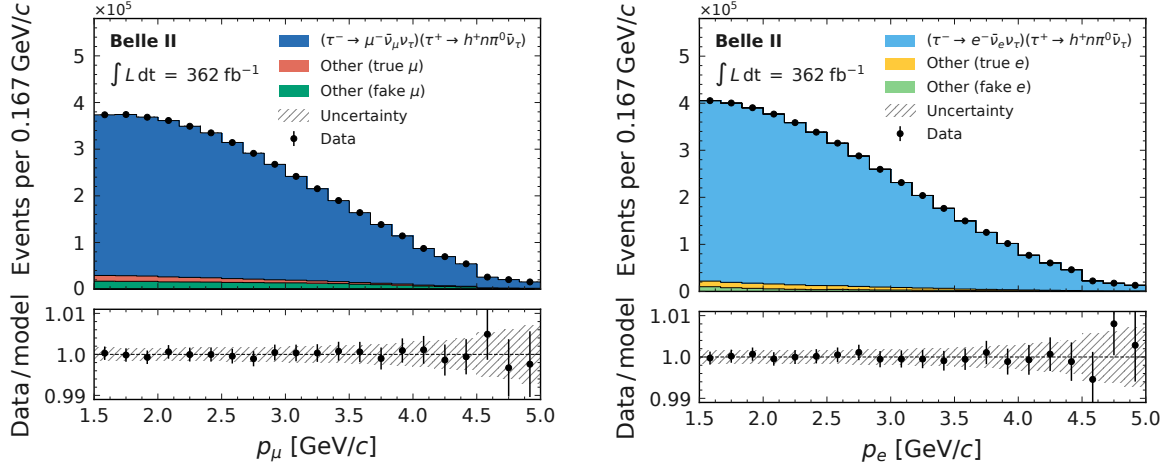


Figure 6. Observed momentum distribution for muon (left) and electron (right) candidates with fit results overlaid. The lower panel shows the ratio between data and fit results. The hatched area indicates the possible variation of the fitted yields due to systematic effects, with the constraints of the nuisance parameters reduced to their fit uncertainties and correlations taken into account.

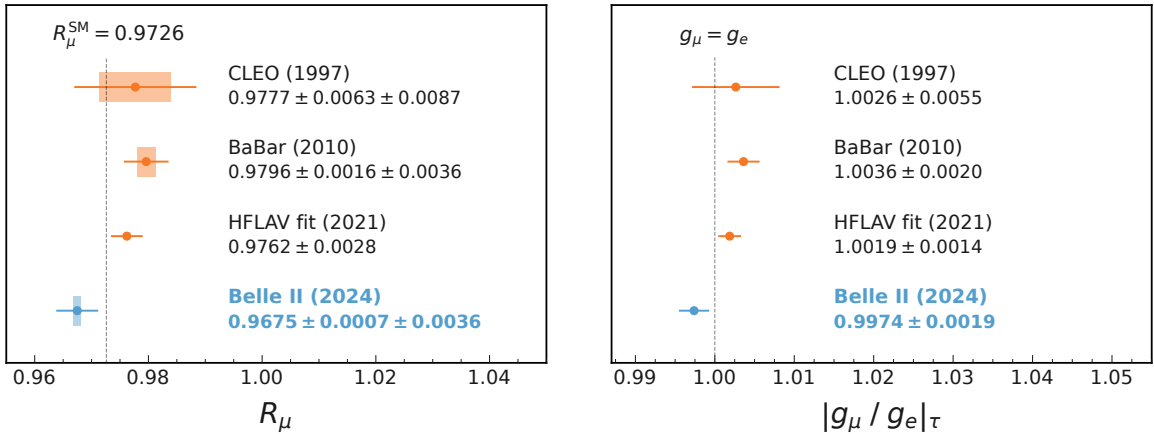


Figure 7. Determinations of R_μ (left) and $|g_\mu/g_e|_\tau$ (right) from previous individual measurements [11, 12] and the fit from the Heavy Flavor Averaging Group [15], compared with the result of this work. The shaded areas represent the statistical uncertainties, while the error bars indicate the total uncertainties. The vertical dashed line indicates the SM prediction, including mass effects.

7 Summary

We report a test of light-lepton universality in leptonic τ decays using a $362 \pm 2 \text{ fb}^{-1}$ sample of data collected by the Belle II detector at the SuperKEKB e^+e^- collider at a centre-of-mass energy of 10.58 GeV. Our result is currently the world's most precise test of light-lepton universality in τ decays performed by a single experiment and is consistent with the SM.

Acknowledgments

This work, based on data collected using the Belle II detector, which was built and commissioned prior to March 2019, was supported by Higher Education and Science Committee of the Republic of Armenia Grant No. 23LCG-1C011; Australian Research Council and Research Grants No. DP200101792, No. DP210101900, No. DP210102831, No. DE220100462, No. LE210100098, and No. LE230100085; Austrian Federal Ministry of Education, Science and Research, Austrian Science Fund No. P 34529, No. J 4731, No. J 4625, and No. M 3153, and Horizon 2020 ERC Starting Grant No. 947006 “InterLeptons”; Natural Sciences and Engineering Research Council of Canada, Compute Canada and CANARIE; National Key R&D Program of China under Contract No. 2022YFA1601903, National Natural Science Foundation of China and Research Grants No. 11575017, No. 11761141009, No. 11705209, No. 11975076, No. 12135005, No. 12150004, No. 12161141008, and No. 12175041, and Shandong Provincial Natural Science Foundation Project ZR2022JQ02; the Czech Science Foundation Grant No. 22-18469S and Charles University Grant Agency project No. 246122; European Research Council, Seventh Framework PIEF-GA-2013-622527, Horizon 2020 ERC-Advanced Grants No. 267104 and No. 884719, Horizon 2020 ERC-Consolidator Grant No. 819127, Horizon 2020 Marie Skłodowska-Curie Grant Agreement No. 700525 “NIOBE” and No. 101026516, and Horizon 2020 Marie Skłodowska-Curie RISE project JENNIFER2 Grant Agreement No. 822070 (European grants); L’Institut National de Physique Nucléaire et de Physique des Particules (IN2P3) du CNRS and L’Agence Nationale de la Recherche (ANR) under grant ANR-21-CE31-0009 (France); BMBF, DFG, HGF, MPG, and AvH Foundation (Germany); Department of Atomic Energy under Project Identification No. RTI 4002, Department of Science and Technology, and UPES SEED funding programs No. UPES/R&D-SEED-INFRA/17052023/01 and No. UPES/R&D-SOE/20062022/06 (India); Israel Science Foundation Grant No. 2476/17, U.S.-Israel Binational Science Foundation Grant No. 2016113, and Israel Ministry of Science Grant No. 3-16543; Istituto Nazionale di Fisica Nucleare and the Research Grants BELLE2; Japan Society for the Promotion of Science, Grant-in-Aid for Scientific Research Grants No. 16H03968, No. 16H03993, No. 16H06492, No. 16K05323, No. 17H01133, No. 17H05405, No. 18K03621, No. 18H03710, No. 18H05226, No. 19H00682, No. 20H05850, No. 20H05858, No. 22H00144, No. 22K14056, No. 22K21347, No. 23H05433, No. 26220706, and No. 26400255, and the Ministry of Education, Culture, Sports, Science, and Technology (MEXT) of Japan; National Research Foundation (NRF) of Korea Grants No. 2016R1D1A1B02012900, No. 2018R1A2B-3003643, No. 2018R1A6A1A06024970, No. 2019R1I1A3A01058933, No. 2021R1A6A1A-03043957, No. 2021R1F1A1060423, No. 2021R1F1A1064008, No. 2022R1A2C1003993, and No. RS-2022-00197659, Radiation Science Research Institute, Foreign Large-Size Research Facility Application Supporting project, the Global Science Experimental Data Hub Center of the Korea Institute of Science and Technology Information and KREONET/GLORIAD; Universiti Malaya RU grant, Akademi Sains Malaysia, and Ministry of Education Malaysia; Frontiers of Science Program Contracts No. FOINS-296, No. CB-221329, No. CB-236394, No. CB-254409, and No. CB-180023, and SEP-CINVESTAV Research Grant No. 237 (Mexico); the Polish Ministry of Science and Higher Education and the National Science Center; the Ministry of Science and Higher Education of the Russian Federation and the

HSE University Basic Research Program, Moscow; University of Tabuk Research Grants No. S-0256-1438 and No. S-0280-1439 (Saudi Arabia); Slovenian Research Agency and Research Grants No. J1-9124 and No. P1-0135; Agencia Estatal de Investigacion, Spain Grant No. RYC2020-029875-I and Generalitat Valenciana, Spain Grant No. CIDEGENT/2018/020; National Science and Technology Council, and Ministry of Education (Taiwan); Thailand Center of Excellence in Physics; TUBITAK ULAKBIM (Turkey); National Research Foundation of Ukraine, Project No. 2020.02/0257, and Ministry of Education and Science of Ukraine; the U.S. National Science Foundation and Research Grants No. PHY-1913789 and No. PHY-2111604, and the U.S. Department of Energy and Research Awards No. DE-AC06-76RLO1830, No. DE-SC0007983, No. DE-SC0009824, No. DE-SC0009973, No. DE-SC0010007, No. DE-SC0010073, No. DE-SC0010118, No. DE-SC0010504, No. DE-SC0011784, No. DE-SC0012704, No. DE-SC0019230, No. DE-SC0021274, No. DE-SC0021616, No. DE-SC0022350, No. DE-SC0023470; and the Vietnam Academy of Science and Technology (VAST) under Grants No. NVCC.05.12/22-23 and No. DL0000.02/24-25.

These acknowledgements are not to be interpreted as an endorsement of any statement made by any of our institutes, funding agencies, governments, or their representatives.

We thank the SuperKEKB team for delivering high-luminosity collisions; the KEK cryogenics group for the efficient operation of the detector solenoid magnet; the KEK Computer Research Center for on-site computing support; the NII for SINET6 network support; and the raw-data centers hosted by BNL, DESY, GridKa, IN2P3, INFN, and the University of Victoria.

References

- [1] Y.-S. Tsai, *Decay correlations of heavy leptons in $e^+ + e^- \rightarrow l^+ + l^-$* , *Phys. Rev. D* **4** (1971) 2821.
- [2] M. Jung, A. Pich and P. Tuzón, *Charged-Higgs phenomenology in the aligned two-Higgs-doublet model*, *J. High Energy Phys.* **11** (2010) 003.
- [3] A. Crivellin, F. Kirk, C.A. Manzari and L. Panizzi, *Searching for lepton flavor universality violation and collider signals from a singly charged scalar singlet*, *Phys. Rev. D* **103** (2021) 073002.
- [4] PiENU collaboration, *Improved Measurement of the $\pi \rightarrow e\nu$ Branching Ratio*, *Phys. Rev. Lett.* **115** (2015) 071801.
- [5] NA62 collaboration, *Precision Measurement of the Ratio of the Charged Kaon Leptonic Decay Rates*, *Phys. Lett. B* **719** (2013) 326.
- [6] KLOE collaboration, *Precise measurement of $\Gamma(K \rightarrow e\nu(\gamma))/\Gamma(K \rightarrow \mu\nu(\gamma))$ and study of $K \rightarrow e\nu\gamma$* , *Eur. Phys. J. C* **64** (2009) 627.
- [7] BELLE collaboration, *Measurement of $\mathcal{R}(D)$ and $\mathcal{R}(D^*)$ with a semileptonic tagging method*, *Phys. Rev. Lett.* **124** (2020) 161803.
- [8] LHCb collaboration, *Measurement of the ratios of branching fractions $\mathcal{R}(D^*)$ and $\mathcal{R}(D^0)$* , *Phys. Rev. Lett.* **131** (2023) 111802.
- [9] ATLAS collaboration, *Test of the universality of τ and μ lepton couplings in W -boson decays with the ATLAS detector*, *Nature Phys.* **17** (2021) 813.

- [10] CMS collaboration, *Precision measurement of the W boson decay branching fractions in proton-proton collisions at $\sqrt{s} = 13$ TeV*, *Phys. Rev. D* **105** (2022) 072008.
- [11] CLEO collaboration, *Experimental test of lepton universality in tau decay*, *Phys. Rev. D* **55** (1997) 2559.
- [12] BABAR collaboration, *Measurements of Charged Current Lepton Universality and $|V_{us}|$ using Tau Lepton Decays to $e^-\bar{\nu}_e\nu_\tau$, $\mu^-\bar{\nu}_\mu\nu_\tau$, $\pi^-\nu_\tau$, and $K^-\nu_\tau$* , *Phys. Rev. Lett.* **105** (2010) 051602.
- [13] W. Altmannshofer, C. Chen, P.S.B. Dev and A. Soni, *Lepton flavor violating Z' explanation of the muon anomalous magnetic moment*, *Phys. Lett. B* **762** (2016) 389.
- [14] D. Bryman, V. Cirigliano, A. Crivellin and G. Inguglia, *Testing Lepton Flavor Universality with Pion, Kaon, Tau, and Beta Decays*, *Ann. Rev. Nucl. Part. Sci.* **72** (2022) 69.
- [15] HEAVY FLAVOR AVERAGING GROUP collaboration, *Averages of b-hadron, c-hadron, and τ -lepton properties as of 2021*, *Phys. Rev. D* **107** (2023) 052008.
- [16] BELLE II collaboration, *Belle II technical design report*, [1011.0352](#).
- [17] K. Akai, K. Furukawa and H. Koiso, *Superkekb collider*, *Nucl. Instrum. Methods Phys. Res. A* **907** (2018) 188.
- [18] S. Jadach, B.F.L. Ward and Z. Wąs, *The precision Monte Carlo event generator KK for two-fermion final states in e^+e^- collisions*, *Comput. Phys. Commun.* **130** (2000) 260.
- [19] S. Jadach, B.F.L. Ward and Z. Wąs, *Coherent exclusive exponentiation for precision Monte Carlo calculations*, *Phys. Rev. D* **63** (2001) 113009.
- [20] S. Banerjee, D. Biswas, T. Przedzinski and Z. Was, *Monte Carlo Event Generator updates, for τ pair events at Belle II energies*, in *16th International Workshop on Tau Lepton Physics*, 11, 2021 [[2111.05914](#)].
- [21] O. Shekhovtsova, T. Przedzinski, P. Roig and Z. Wąs, *Resonance chiral Lagrangian currents and τ decay Monte Carlo*, *Phys. Rev. D* **86** (2012) 113008.
- [22] M. Chruszcz, T. Przedzinski, Z. Wąs and J. Zaremba, *TAUOLA of τ lepton decays—framework for hadronic currents, matrix elements and anomalous decays*, *Comput. Phys. Commun.* **232** (2018) 220.
- [23] I.M. Nugent, T. Przedzinski, P. Roig, O. Shekhovtsova and Z. Wąs, *Resonance chiral Lagrangian currents and experimental data for $\tau^- \rightarrow \pi^-\pi^-\pi^+\nu_\tau$* , *Phys. Rev. D* **88** (2013) 093012.
- [24] E. Barberio, B. van Eijk and Z. Wąs, *PHOTOS: A universal Monte Carlo for QED radiative corrections in decays*, *Comput. Phys. Commun.* **66** (1991) 115.
- [25] T. Sjöstrand, S. Ask, J.R. Christiansen, R. Corke, N. Desai, P. Ilten et al., *An Introduction to PYTHIA 8.2*, *Comput. Phys. Commun.* **191** (2015) 159.
- [26] G. Balossini, C.M. Carloni Calame, G. Montagna, O. Nicrosini and F. Piccinini, *Matching perturbative and parton shower corrections to Bhabha process at flavour factories*, *Nucl. Phys. B* **758** (2006) 227.
- [27] G. Balossini, C. Bignamini, C.M.C. Calame, G. Montagna, O. Nicrosini and F. Piccinini, *Photon pair production at flavour factories with per mille accuracy*, *Phys. Lett. B* **663** (2008) 209.
- [28] C.M. Carloni Calame, G. Montagna, O. Nicrosini and F. Piccinini, *The BABAYAGA event generator*, *Nucl. Phys. B Proc. Suppl.* **131** (2004) 48.

- [29] C.M. Carloni Calame, *An improved parton shower algorithm in QED*, *Phys. Lett. B* **520** (2001) 16.
- [30] C.M. Carloni Calame, C. Lunardini, G. Montagna, O. Nicrosini and F. Piccinini, *Large angle Bhabha scattering and luminosity at flavor factories*, *Nucl. Phys. B* **584** (2000) 459.
- [31] F. Berends, P. Daverveldt and R. Kleiss, *Radiative corrections to the process $e^+e^- \rightarrow e^+e^-\mu^+\mu^-$* , *Nucl. Phys. B* **253** (1985) 421.
- [32] F. Berends, P. Daverveldt and R. Kleiss, *Complete lowest-order calculations for four-lepton final states in electron-positron collisions*, *Nucl. Phys. B* **253** (1985) 441.
- [33] F. Berends, P. Daverveldt and R. Kleiss, *Monte Carlo simulation of two-photon processes: II: Complete lowest order calculations for four-lepton production processes in electron-positron collisions*, *Comp. Phys. Commun.* **40** (1986) 285.
- [34] S. Uehara, *TREPS: A Monte-Carlo Event Generator for Two-photon Processes at e^+e^- Colliders using an Equivalent Photon Approximation*, [1310.0157](https://arxiv.org/abs/1310.0157).
- [35] BELLE II FRAMEWORK SOFTWARE GROUP collaboration, *The Belle II Core Software*, *Comput. Softw. Big Sci.* **3** (2019) 1.
- [36] BELLE II collaboration, “Belle II Analysis Software Framework (basf2).” <https://doi.org/10.5281/zenodo.5574115>.
- [37] GEANT4 collaboration, *GEANT4: A simulation toolkit*, *Nucl. Instrum. Methods Phys. Res. A* **506** (2003) 250.
- [38] S. Brandt, C. Peyrou, R. Sosnowski and A. Wroblewski, *The Principal axis of jets. An Attempt to analyze high-energy collisions as two-body processes*, *Phys. Lett.* **12** (1964) 57.
- [39] E. Farhi, *A QCD Test for Jets*, *Phys. Rev. Lett.* **39** (1977) 1587.
- [40] M. Milesi, J. Tan and P. Urquijo, *Lepton identification in Belle II using observables from the electromagnetic calorimeter and precision trackers*, *EPJ Web Conf.* **245** (2020) 06023.
- [41] PARTICLE DATA GROUP collaboration, *Review of Particle Physics*, *PTEP* **2022** (2022) 083C01.
- [42] I.J. Good, *Rational Decisions*, *J. R. Stat. Soc. Series B Stat. Methodol.* **14** (2018) 107.
- [43] A. Paszke, S. Gross, F. Massa, A. Lerer, J. Bradbury, G. Chanan et al., *Pytorch: An imperative style, high-performance deep learning library*, [1912.01703](https://arxiv.org/abs/1912.01703).
- [44] L. Heinrich, M. Feickert, G. Stark and K. Cranmer, *pyhf: pure-Python implementation of HistFactory statistical models*, *J. Open Source Softw.* **6** (2021) 2823.
- [45] ROOT collaboration, K. Cranmer, G. Lewis, L. Moneta, A. Shibata and W. Verkerke, *HistFactory: A tool for creating statistical models for use with RooFit and RooStats*, 2012. 10.17181/CERN-OPEN-2012-016.